

Ab initio molecular dynamics calculations of ion hydration free energies

Kevin Leung^{*}, Susan B. Rempe, and O. Anatole von Lilienfeld

Citation: *The Journal of Chemical Physics* **130**, 204507 (2009); doi: 10.1063/1.3137054

View online: <http://dx.doi.org/10.1063/1.3137054>

View Table of Contents: <http://aip.scitation.org/toc/jcp/130/20>

Published by the *American Institute of Physics*

COMPLETELY

REDESIGNED!



**PHYSICS
TODAY**

Physics Today Buyer's Guide
Search with a purpose.

Ab initio molecular dynamics calculations of ion hydration free energiesKevin Leung,^{1,a)} Susan B. Rempe,² and O. Anatole von Lilienfeld³¹*Department of Surface and Interface Sciences, MS 1415, Sandia National Laboratories, Albuquerque, New Mexico 87185, USA*²*Department of Nanobiology, MS 0895, Sandia National Laboratories, Albuquerque, New Mexico 87185, USA*³*Department of Multiscale Dynamic Materials Modeling, MS 1322, Sandia National Laboratories, Albuquerque, New Mexico 87185, USA*

(Received 12 February 2009; accepted 25 April 2009; published online 27 May 2009)

We apply *ab initio* molecular dynamics (AIMD) methods in conjunction with the thermodynamic integration or “ λ -path” technique to compute the intrinsic hydration free energies of Li^+ , Cl^- , and Ag^+ ions. Using the Perdew–Burke–Ernzerhof functional, adapting methods developed for classical force field applications, and with consistent assumptions about surface potential (ϕ) contributions, we obtain absolute AIMD hydration free energies (ΔG_{hyd}) within a few kcal/mol, or better than 4%, of Tissandier *et al.*'s [J. Phys. Chem. A **102**, 7787 (1998)] experimental values augmented with the SPC/E water model ϕ predictions. The sums of Li^+/Cl^- and Ag^+/Cl^- AIMD ΔG_{hyd} , which are not affected by surface potentials, are within 2.6% and 1.2 % of experimental values, respectively. We also report the free energy changes associated with the transition metal ion redox reaction $\text{Ag}^+ + \text{Ni}^+ \rightarrow \text{Ag} + \text{Ni}^{2+}$ in water. The predictions for this reaction suggest that existing estimates of ΔG_{hyd} for unstable radiolysis intermediates such as Ni^+ may need to be extensively revised. © 2009 American Institute of Physics. [DOI: [10.1063/1.3137054](https://doi.org/10.1063/1.3137054)]

I. INTRODUCTION

Accurate predictions of hydration free energies of ions and molecules are crucial for modeling chemical and biochemical reactions in water and the adsorption of ionic species at water-material interfaces and inside nanopores.¹ State-of-the-art density functional theory (DFT)-based *ab initio* molecular dynamics (AIMD) simulations allow modeling the breaking and making of chemical bonds, as well as molecular polarizability. Direct use of AIMD to predict ion hydration free energies, ΔG_{hyd} , will have significant impact on computational electrochemistry, biophysics, desalination, energy storage applications, corrosion studies, and geochemistry. AIMD simulations have already been extensively applied to study the hydration structure of ions,^{2–5} in many cases, leading to more accurate predictions of the hydration number than classical force field methods. At the same time, using hydration structure information and DFT and quantum chemistry calculations, the quasichemical method has been applied to predict highly accurate ΔG_{hyd} for ions in water and biological binding sites.⁶ In this manuscript, we generalize and apply ΔG_{hyd} methods developed for classical force fields to AIMD simulations. In some cases, our work can be related to “alchemical” potentials within the context of molecular grand-canonical ensemble DFT that allows variations of atomic numbers and electron numbers.⁷

Many of the techniques we use for predicting AIMD ΔG_{hyd} have non-DFT precedents. In classical force field treatments of hydrated ions, ΔG_{hyd} at infinite ion dilution has been successfully computed^{8–11} using the thermodynamic integration (TI) method,^{12,13}

$$\Delta G_{\text{hyd}} = \int_0^1 d\lambda \left\langle \frac{dH(\lambda)}{d\lambda} \right\rangle_{\lambda}, \quad (1)$$

or free energy perturbation¹⁴ and closely related techniques. Here $0 \leq \lambda \leq 1$ interpolates between the initial and final systems, $H(\lambda)$ is the Hamiltonian as λ varies, the brackets denote equilibrium sampling with the Boltzmann factor $\exp[-\beta H(\lambda)]$, and $\beta = 1/k_{\text{B}}T$. For obvious reasons, the method is also called “ λ -path integration.”⁷ ΔG_{hyd} is a state property, independent of the interpolation pathway. Force field parameters for ions are generally fitted with a specific water model [e.g., SPC/E (Ref. 15)] to reproduce experimental ΔG_{hyd} values. In simulations of monatomic ions M with charge q , λ is conveniently set to be proportional to q in Eq. (1) such that the ion is “charged up” linearly from M^0 to M^{q+} .

Two critical theoretical advances have enabled direct comparisons of predicted ΔG_{hyd} with tabulated data. (A) The long-range nature of Coulomb interactions means a significant simulation cell size dependence arises when using Ewald summations.¹⁶ This dependence derives from the interactions of an ion with its images as well as with the neutralizing background in a charged simulation cell. To remove this dependence, Hummer *et al.* devised a monopole correction so effective that even an eight-water simulation cell containing a Na^+ ion already yields ΔG_{hyd} well converged with system size.^{8,9} (B) Comparison with experiments effectively entails bringing an ion from vacuum at infinity into the bulk liquid water region. A surface potential, ϕ , materializes at the liquid-vapor interface, leading to a shift in the ion free energy $q\phi$ in the aqueous phase.^{17–19} Accounting for the sur-

^{a)}Electronic mail: kleung@sandia.gov.

face potential, the calculated absolute ion hydration free energy, which may not be measurable,¹⁷ becomes

$$\Delta G_{\text{tot}} = \Delta G_{\text{Ewald}} + q(\phi_d + \phi_q). \quad (2)$$

Here ΔG_{Ewald} is the hydration free energy computed using standard Ewald summation which assumes a zero average electrostatic potential inside the simulation cell.²⁰ ϕ_d and ϕ_q are the dipolar and quadrupolar (or “spherical second moment”) contributions to the surface potential ϕ . Some reported experimental data have subtracted the effect of this potential²¹ while others have not.²²

The rapid convergence of ΔG_{hyd} with simulation cell size (A) significantly facilitates the application of this ΔG_{hyd} formalism to computationally costly DFT-based AIMD simulations. Special attention should be paid to the surface potential contribution (B) in AIMD settings. Unlike classical models for water, $\phi = \phi_d + \phi_q$ has not yet been predicted for AIMD water [e.g., computed with a generalized-gradient approximated (GGA) Kohn–Sham functional such as Perdew–Burke–Ernzerhof²³ (PBE)]. Such a calculation would entail a large simulation cell depicting the interface and long sampling trajectories. Furthermore, as the liquid water density affects ϕ_q ,^{17–19,24} the effectiveness of such a calculation may further be limited by the fact that bulk GGA water may not exhibit 1.0 g/cm³ density.^{25,26} Although ϕ_d and ϕ_q are not independent—they require a common choice of molecular center, typically taken to be the oxygen atom of water molecules—the quantity ϕ_q has recently been computed for PBE water using maximally localized Wannier functions.¹⁹ This piece of information is important for DFT-based calculations because ΔG_{Ewald} itself is an ambiguous quantity whose value depends on whether the pseudopotential (PP) contains core electrons, while $\Delta G_{\text{Ewald}} + q\phi_q$ is independent of such DFT details. We therefore redefine

$$\Delta G_{\text{hyd}} = \Delta G_{\text{Ewald}} + q\phi_q. \quad (3)$$

To further enable comparison with experimental data in Ref. 21, which contain no surface potential contributions, we add $q\phi_q = -19.7q$ kcal/mol, the quadrupole moment value for SPC/E water at 1.00 g/cm³ density when the oxygen site is chosen as the molecular center. This is appropriate because ΔG_{hyd} for various ions have been fitted to Ref. 21 using the SPC/E water model¹⁰ or the very similar SPC model.^{8,9} In effect, we are comparing AIMD ΔG_{hyd} with *SPC/E calculations fitted to the data* of Ref. 21. For the data tabulated in Ref. 22, which contain the surface potential term $q(\phi_d + \phi_q)$, we subtract $q\phi_d = 4.8q$ kcal/mol estimated using SPC/E water model-based water-vapor interface molecular dynamics calculations.¹⁸ Although an investigation of ϕ_d predicted with different methods is not the focus of this work, accurate DFT methods and accurate force fields should yield similar, reliable ϕ_d . Even if there exists a 50% uncertainty in this SPC/E ϕ_d estimate, $\Delta G_{\text{hyd}} + q\phi_d$ in water will be affected by only $\sim 2.4|q|$ kcal/mol. Indeed, the much used SPC and the TIP4P water models yield $\phi_d = 5.5$ and 7.1 kcal/mol/ $|e|$, respectively,^{27–29} which are slightly different from the SPC/E ϕ_d . The discrepancies among these models can be taken as a measure of the systematic uncertainty associated with our ϕ_d assignments.

Finally, experimental data for moving ions from vacuum into aqueous solution are referenced to their respective standard states, i.e., gas phase ions at 1.0 atm. pressure and hydrated ions at 1.0M concentration. To be consistent with the infinite dilution limit ΔG_{hyd} predicted in this work, $C^{(0)} = 1.9$ kcal/mol is further subtracted from tabulated ΔG_{Tiss} for all ions regardless of their charges to account for the volume change included in the experimental data. Due to a sign problem,⁶ $2C^{(0)}$ kcal/mol needs to be subtracted from ΔG_{Marcus} for this purpose.

To summarize, we compare our AIMD ΔG_{hyd} [Eq. (3)] with $\Delta G_{\text{Marcus}} + q\phi_q^{\text{SPC/E}} - 2C^{(0)}$ kcal/mol and $\Delta G_{\text{Tiss}} - q\phi_d^{\text{SPC/E}} - C^{(0)}$ kcal/mol, where ΔG_{Marcus} and ΔG_{Tiss} are the values listed in Refs. 21 and 22, respectively.

Note that the proton is often used as a reference for hydration free energies.³⁰ Referencing the predicted ΔG_{hyd} of ions with that of H⁺ computed in the same way circumvents the need to estimate ϕ . In AIMD settings, however, an excess proton can migrate from one H₂O to another. Therefore we have not yet attempted to compute this proton ΔG_{hyd} .

For test cases, we consider Li⁺ and Cl[−]. The Li⁺ ion hydration structure and hydration free energies have been extensively studied using AIMD and quasichemical methods, respectively.³ Computing the ΔG_{hyd} of Cl[−] further allows us to predict the summed ΔG_{hyd} of the monovalent Li⁺/Cl[−] pair, where the surface potential terms cancel and the result contains less systematic uncertainty. We show that this summed value is at worst within 2.6% of experimental results.^{21,22}

We also study the change in hydration free energies associated with



and the corresponding electrochemical half cell reactions,



and



These reactions are pertinent not only to elementary electrochemical processes, but also to the initial stages of nanoalloy synthesis by radiolysis.^{31,32} γ irradiation of mixed electrolytic aqueous solutions releases secondary electrons that reduce the metal ions to atoms or lower oxidation state ions. These reduced species readily coalesce to form clusters. In the case of a mixed Ag(I)/Ni(II) solution, the exothermicity of Eq. (4) will determine whether reduced Ni species are readily reoxidized by Ag⁺ in the solution—a side reaction that hinders nanoalloy cluster formation. AIMD is an attractive route to estimate the redox free energies associated with Ni(I) species, which exhibit short lifetimes and are difficult to probe experimentally.

Apart from the ability to compare AIMD ΔG_{hyd} with quasichemical theory^{6,33} and potentially extend DFT-based absolute hydration free energy calculations to inhomogeneous media, this work is important due to its close relationship to recent theoretical advances. One is the alchemical λ -path integration technique recently formulated within a DFT/AIMD-based molecular grand-canonical ensemble scheme,⁷ which accounts for changes in PPs as well as the

number of electrons. As long as the PP replaces all core electrons in the ion, ΔG_{hyd} TI calculations are very similar within AIMD and the SPC/E model treatments of water. More complex treatments are required, however, when ion insertion into the solvent involves not only changes in the ionic PP but also injection of electrons.⁷ This alchemical path technique has been applied to quantum mechanics/molecular mechanics (QM/MM) simulations of electron transfer reactions of aqueous metal complexes [Fe(II/III) and Ru(II/III)].³⁴ Our work is even more closely related to purely AIMD-based computational electrochemistry.³⁵ Here the electron transfer processes are similar to those in Ref. 34, but all water molecules are treated with DFT methods, and the long-range electrostatics are fundamentally different from those in QM/MM calculations. Our computational approach treats the ionization potential and the ion hydration free energy contributions to the redox potential separately. While it is based on and derives its rigor from theories well established with classical force field hydration treatments [e.g., Eq. (3)], our thermodynamic method has not been extended to estimate the fluctuating gaps that are necessary for calculating reaction rates via the Marcus theory.³⁵

II. METHOD

A. VASP calculations

We apply the Vienna atomistic simulation package³⁶ (VASP) version 4.6 with a modified pot.F,¹⁹ the PBE exchange correlation functional,²³ projected-augmented wave (PAW) PPs (Refs. 37 and 38) with only valence electrons for Li, Cl, H, and O atoms, and Ag and Ni PPs that include pseudovalent $4p$ and $3p$ electrons. Two protocols to generate VASP AIMD trajectories for Li^+ solvated in water are applied. For the ion plus 32-water simulations, we use a cell size of 9.855 Å corresponding to a water density of 1.0 g/cm³, a 0.25 fs time step, an energy cutoff of 400 eV, and a Born–Oppenheimer convergence of 10^{-6} eV at each time step. For 64-water simulations, the corresponding parameters are 12.417 Å (1.0 g/cm³), 0.5 fs, 500 eV, and 10^{-7} eV, respectively. These settings limit the temperature drifts to 1 and 0.5 K/ps, respectively. The trajectory length for each value of q is at least 40 ps in two-point TI calculations and at least 30 ps for six-point TI. Initial configurations are pre-equilibrated using the SPC/E water model and ion force fields¹⁰ with charges scaled to the net charge of the corresponding AIMD simulation cells. A Nose thermostat is applied, setting $T = 400$ K, which is needed for the PBE functional to describe experimental liquid water at room temperature.³⁹ The deuterium mass is adopted for all protons to allow a larger time step, although the H mass is assumed whenever water density is reported. Ag^+ and Ni^{2+} simulations are performed at 0.99 g/cm³ water density while the Cl^- simulation is at 1.0 g/cm³ density; these simulation cells all contain 32 H_2O molecules, and the time step, energy cutoff, and convergence criteria used are analogous to those for $\text{Li}^+ / 32 \text{H}_2\text{O}$.

B. Visualizing electronic isosurfaces

Electronic isosurfaces and integrated changes in electron density, $\Delta(x) = \int dydz [\rho(x, y, z)_n - \rho(x, y, z)_c]$ as functions of

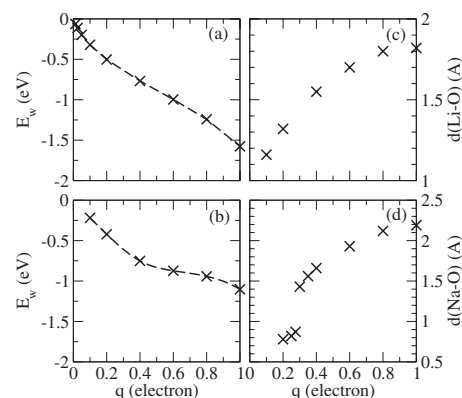


FIG. 1. The binding energies and optimized distances between a H_2O molecule and VASP PBE PPs globally scaled by a factor of $0 < q \leq 1$. [(a) and (c)] Li^+ ; [(b) and (d)] Na^+ . The PPs have no core electrons. Dashed lines are cubic spline fits. Na^+ is meant as a counter example to Li^+ for gas phase behavior; its behavior in water will not be the focus of this work.

spatial coordinate x , are also computed and depicted for Li^{q+} in water for various values of q . The depicted geometries are snapshots taken at the end of the 32-water PBE simulations. These results are obtained using the code CPMD,⁴⁰ the PBE functional,²³ PPs from Ref. 41, and a cutoff of 100 Ry (1361 eV). ρ_c refers to the electron density obtained by minimizing the energy within the indicated charge. As with VASP, CPMD uses an opposite background charge to neutralize the system within the periodically replicated simulation cells. ρ_n corresponds to the density of the same geometry but with the charged species replaced by a neutral He atom.

C. Li^+ thermodynamic integration

To implement Eq. (1) for Li^+ , we generate integrand values at different q values according to two different integration formulas: A two-point Gaussian quadrature and a six-point trapezoidal rule. To that end, AIMD trajectories apply a Li^+ PP (which contains no core electrons) globally scaled by Gaussian quadrature values $q = 0.211\ 325$ and $0.788\ 675$. This procedure is analogous to the scaling of the ionic charges in classical force field molecular dynamics calculations of hydration free energies.³³ In addition, $q = 0.1, 0.4, 0.6,$ and 1.0 are considered. Using these six points, a cubic least-squared fit is applied to extrapolate the integrand value to $q = 0$.⁴² These steps yield six almost evenly spaced integration points needed to implement a trapezoidal rule integration.

Figure 1(a) shows that the scaled VASP Li^+ PP behaves to some extent like a classical force field Li^{q+} ; its binding energy with one H_2O molecule scales roughly linearly with q except at very small q . The optimal $\text{Li}-\text{O}_{\text{water}}$ distance also shrinks smoothly with decreasing q [Fig. 1(c)]. In contrast, Fig. 1(b) shows that the scaled VASP PBE Na^+ exhibits water binding energies that deviate more strongly from linearity. Furthermore, the optimal q -scaled Na^+-OH_2 distance sharply decreases to 0.87 Å at $q \approx 0.29$, which suggests the formation of an anomalous covalent bond beyond $q < 0.29$ [Fig. 1(d)]. For efficient AIMD ΔG_{hyd} simulations, a pathway should be chosen such that at the selected simulation

points, electron transfer or unphysical chemical bonding between the scaled PP and H₂O is avoided.

The AIMD trajectory is sampled every 0.1 ps. At such intervals, we use a finite difference method to compute $dH(q)/dq = [H(q+\Delta q/2) - H(q-\Delta q/2)]/q$ at fixed atomic configurations. Here $H(q)$ is the total potential energy of the simulation cell predicted using VASP. When taking finite derivatives, Δq values of 0.025 and 0.050 yield Li⁺ hydration free energies that agree to within 0.5 kcal/mol. Evaluating $\langle dH(q)/dq \rangle_q$ using 400 eV and 500 eV cutoffs lead to indistinguishable results.

The derivative is corrected for finite size effects by adding the Ewald correction to the energy $\alpha q^2/2L$ at each q , where α is the Madelung constant, to the Li⁺-plus-water VASP energies [issue “(A)” discussed in the introduction⁸]. The quadrupole moment correction $q\phi_q$ is linearly dependent on q and has been estimated in Ref. 19. With the slightly smaller simulation cell used in this work, the ϕ_q corrections are predicted to be 3.85 and 3.81 eV for 1.00 and 0.99 g/cm³ water density.⁴³ Unlike classical force field calculations, the isolated ion Li^{q+} carries a nonzero energy. Thus we subtract $(dH_{\text{bare ion}}(q)/dq)_q$ from Eq. (1).

Unless otherwise noted, the Li⁺ thermodynamic integration protocol (e.g., the sampling interval, subtraction of bare ion energies) is applied to all other ions.

D. Cl⁻ thermodynamic integration

ΔG_{hyd} for Cl⁻ requires a different TI procedure. Unlike the Li⁺ PP without explicit 1s electrons, scaling the VASP Cl⁻ PP to zero also involves removing eight electrons. While it is possible to alchemically perturb Cl⁻ to Ar, this TI route is not directly applicable for multiatom anions. Instead, we first use TI to “grow” a nonpolarizable classical force field¹⁰ (FF) Cl⁻ with a negative point charge and a Lennard-Jones interaction¹⁰ with the oxygen sites of PBE water. This can be regarded as a QM/MM simulation, but with the solvent (not solute) treated quantum mechanically. Then we use a one-step free energy perturbation procedure,

$$\beta[\Delta G(\text{PBE}) - \Delta G(\text{FF})] = -\log\langle \exp[-\beta(H(\text{PBE}) - H(\text{FF}))] \rangle_{\text{FF}}, \quad (7)$$

to estimate the PBE Cl⁻ ΔG_{hyd} . As long as the hydration structures of the classical and PBE ion in PBE water are similar, this method can be generally and accurately applied to multiatom anions or cations, as well as PPs like the VASP PAW PBE Na⁺ whose interaction with water exhibits anomalies when the PP is scaled continuously to zero (Fig. 1). If there are partial positive point charges in the classical force field, however, the DFT valence electrons may collapse onto those atomic sites, and PPs that repel electrons may be needed to prevent such a collapse.

E. Ag⁺ and Ni²⁺ thermodynamic integration

The VASP PBE PPs used for Ag and Ni contain 11 and 16 electrons, respectively. When the number of electrons in 32-water simulation cell is fixed at $(32 \times 8 + 11 - q)$ and $(32 \times 8 + 16 - q)$ in AIMD trajectories, our maximally localized

Wannier function analyses⁴⁴ reveal that $(11-q)$ and $(16-q)$ electrons remain localized on Ag and Ni, respectively. This indicates that Ag^{q+} and Ni^{q+} species exhibit no tendency to eject excess electrons into water,⁴⁵ and the partially charged ions are preserved within a λ -path that vary the total number of electrons in the system. Hence we simply use the number of electrons as the order parameter, λ , analogous to Refs. 7, 34, and 35. $dH(q)/dq$ is simply computed by adding and subtracting 0.025 electrons to the simulation cell and performing a finite difference. The exceptions are Ag⁺ (where we compute the difference between Ag⁺ and Ag^{0.95+}); Ni⁺ (Ni⁺ and Ni^{1.05+}); and Ni²⁺ (Ni^{1.95+} and Ni²⁺). As we subtract the bare ion contribution at each q , the expression $(\langle dH(q)/dq \rangle - (dH_{\text{bare ion}}(q)/dq))$ should reflect purely solvent-induced effects.

For Ag, spin-polarized PBE calculations are adequate. In contrast, spin-polarized PBE-based AIMD simulations of Ni^{q+} in water underestimate the gap between the highest occupied molecular orbital (HOMO) and lowest unoccupied molecular orbital (LUMO). This occurs because PBE severely underestimates exchange interactions in the localized 3d orbitals, leading to near degeneracies in intermediate- q Ni^{q+} d -shell orbitals and slow numerical convergence of the electronic structure at each Born–Oppenheimer AIMD time step. We have therefore applied the DFT+U technique⁴⁶ to the Ni 3d orbitals to generate AIMD trajectories with which we evaluate Eq. (1) using only the PBE functional. Originally devised for solid state applications, DFT+U has recently been adapted for molecular systems and even used in AIMD settings.^{47,48} U is set at 4.0 eV to yield a 15.7 eV gas phase Ni²⁺ binding energy in a Ni²⁺(H₂O)₆ cluster. This is the value predicted using the B3LYP hybrid functional⁴⁹ and a 6-311+G(d,p) basis.⁵⁰ Using DFT+U generated geometries for PBE ΔG_{hyd} is justified because, in the gas phase, the PBE functional and DFT+U predict optimized Ni²⁺(H₂O)₆ geometries which are nearly identical.

III. RESULTS

A. Li⁺ hydration free energy

Figure 2 plots $\langle dH(q)/dq \rangle_q$ as q varies after subtracting contributions from Ewald images,⁸ the quadrupole or spherical second moment contribution $q\phi_q$,¹⁹ and the energies of the bare Li^{q+}. $\langle dH(q)/dq \rangle_q$ computed using 32- and 64-H₂O simulation cells at 1.00 g/cm³ H₂O density are in good agreement at $q=0.21$ and $q=0.79$. Using a two-point Gaussian quadrature, ΔG_{hyd} for the two cells integrate to -128.6 and -126.7 kcal/mol, respectively (Table I). Splitting the data into four segments, the standard deviations in these ΔG_{hyd} are found to be 1.1 and 0.5 kcal/mol, respectively.⁵¹ Thus the two cell sizes exhibit ΔG_{hyd} approximately within numerical uncertainties of each other, showing that the finite system size effect is small for AIMD after applying the Ewald correction, as is the case with classical force field simulations.^{8,9} A dielectric continuum estimate would suggest that, after adding the leading order ($1/L$) Ewald correction, the 32-water simulation cell result is already converged to the infinite dilution limit to within 1 kcal/mol (Ref. 9).

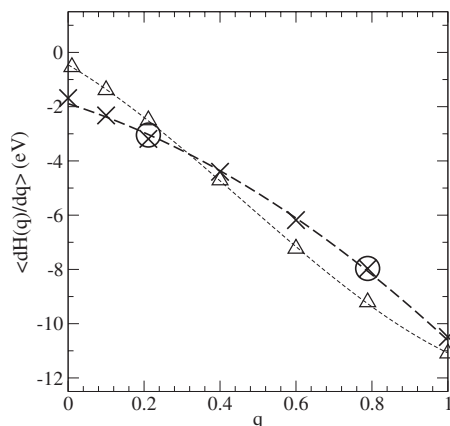


FIG. 2. $\langle dH(q)/dq \rangle_q$ for Li^{q+} as q varies. The bare ion contributions, Ewald corrections, and electrostatic potential shift due to the quadrupole moment have been subtracted. Crosses: 32 H_2O , 1.00 g/cm³; circles: 64 H_2O , 1.00 g/cm³; triangles, same as crosses but are for SPC/E water. The dashed lines are cubic least-squared fits to the crosses and triangles.

For illustrative purposes, we also display in Fig. 3 the Li-ion growth-induced changes in the total electron density integrated over the x - and y -coordinates. From inspection of this change arising from the presence of the increasingly charged ion one can conclude that, as expected, the attraction of electrons toward the ion increases as the charge approaches +1.0. The isosurface plots support a similar conclusion. For small values of q , changes in density occur throughout the system. As q approaches its final value, however, the drastic increase in electronic density at the ion position due to increasingly polarized water [Fig. 3(a)] is hidden behind the large sphere of depleted density. This large sphere comes about because we have subtracted the electron density of a neutral helium atom from that of the Li^+ PP.

Figure 4 depicts the pair correlation functions $g(r)$ between Li^{q+} and the O and H sites in H_2O . Recall that the entire VASP PBE Li^+ PP, including the long-range coulomb and the short-range Pauli-exclusion contributions, is scaled with q . Hence, at small q , the most probable Li^{q+} - O_{water} distance is much reduced from the $q=1$ case. Nevertheless, we have verified that negligible electron density resides near

TABLE I. Li^+ hydration free energies using different computational protocols. H_2O densities and ΔG_{hyd} are in units of g/cm³ and kcal/mol, respectively. Experimental values adjusted for surface potentials and standard state contributions are marked with a dagger (see text).

Ion	N_{water}	ρ_{water}	Quadrature	ΔG_{hyd}
Li^+	32	1.00	2-pt	-128.6
Li^+	32	1.00	6-pt	-128.3
Li^+	64	1.00	2-pt	-126.7
Li^+	32	0.97	2-pt	-126.7
Li^+	32	0.97	6-pt	-127.2
Li^+	SPC/E	1.00	6-pt	-134.9
Li^+	Expt. ^a	1.00	NA	-113.5
Li^+	Expt. ^{a,†}	1.00	NA	-137.0
Li^+	Expt. ^b	1.00	NA	-126.5
Li^+	Expt. ^{b,†}	1.00	NA	-133.2

^aReference 21.

^bReference 22.

the Li^{q+} nuclei, indicating that Li^{q+} does behave like a partially charged ion in water. The insets depict the instantaneous hydration numbers N_w , computed at each time step by integrating each $g_{Li-O}(r)$ to its first minimum. For $q=0.21$, N_w averages only to 1.5 and experiences rapid temporal fluctuations. Despite this, $g_{Li-O}(r)$ still exhibits a high peak value because the scaled Li^{q+} has such a small radius. At $q=0.79$, $N_w=3.5$, approaching the $N_w=4$ AIMD value reported for Li^+ .³

Figure 5 depicts the logarithm of the distributions of instantaneous hydration numbers for $Li^{0.2+}$ and Li^+ . In conjunction with low order m $\langle d^m H(q)/dq^m \rangle$ derivatives, hydration number distributions at the TI end points can, in principle, be used to predict the hydration free energy using a single AIMD trajectory at $q=0$ or $q=1$.⁵² Since we have avoided $q=0$ and the finite differences applied in our implementation may not be accurate for $m>1$, we have not attempted to estimate ΔG_{hyd} with high order derivatives, but have used 2 or 6 q values to evaluate ΔG_{hyd} . Note that, using the quasichemical theoretical framework, hydration number distributions of a solute can be used directly to estimate hydration free energies,⁶ as demonstrated in recent works.^{4,6,54} Furthermore, such distributions are of intrinsic interest and can lend useful comparison with those predicted using classical force field simulations. See also Ref. 55 for other methods devised to reduce the number of q -value integrands needed to perform TI calculations.

We next investigate the accuracy of the two-point TI quadrature by further sampling $\langle dH(q)/dq \rangle_q$ at $q=0.1, 0.4, 0.6, 1.0$ in addition to 0.21 and 0.79 in a simulation cell. This denser grid allows an approximate six-point trapezoidal rule integration after we extrapolate $\langle dH(q)/dq \rangle_q$ to $q=0.0$. Figure 2 shows that $\langle dH(q)/dq \rangle_q$ is almost linear for a large, intermediate q range except near $q=0$ and $q=1$. This is in qualitative agreement with SPC/E model predictions^{9,11} which we also compute for a 32-water simulation cell and depict in Fig. 2. The deviation from linearity at $q=0$ is well reproduced with a cubic fit for both AIMD and SPC/E $\langle dH(q)/dq \rangle_q$. Table I confirms that the two-point and six-point formulas yield ΔG_{hyd} within 0.3 kcal/mol of each other—well within the numerical uncertainties of the simulations. Henceforth we will report the six-point value of $\Delta G_{hyd}=-128.3 \pm 0.9$ kcal/mol for Li^+ .

This success of the two-point formula appears, however, somewhat fortuitous. One would not *a priori* expect this quadrature to be accurate for Li^+ because of the large changes in effective Li^{q+} radius (Fig. 4). The classic Born hydration free energy formula, based on a dielectric continuum description of the solvent, predicts $\Delta G_{Born} \propto q^2/(2a) \times (1-1/\epsilon)$ at a fixed ionic radius a . It is quadratically dependent on q when a is held constant. In nonpolarizable classical force field ΔG_{hyd} simulations, the Lennard-Jones radius of the ion is also held fixed while the ionic charge varies. The constant radius thus seems crucial to the accuracy of the two-point Gaussian quadrature, which is exact only if $\langle dH(q)/dq \rangle_q$ is linear in q . Despite this, the two-point formula will be shown to be accurate for the AIMD ΔG_{hyd} associated with Li^+ , Ag^+ , and $Ni^+ \rightarrow Ni^{2+}$ considered in this work. It appears less accurate for Cl^- , unlike SPC/E-based

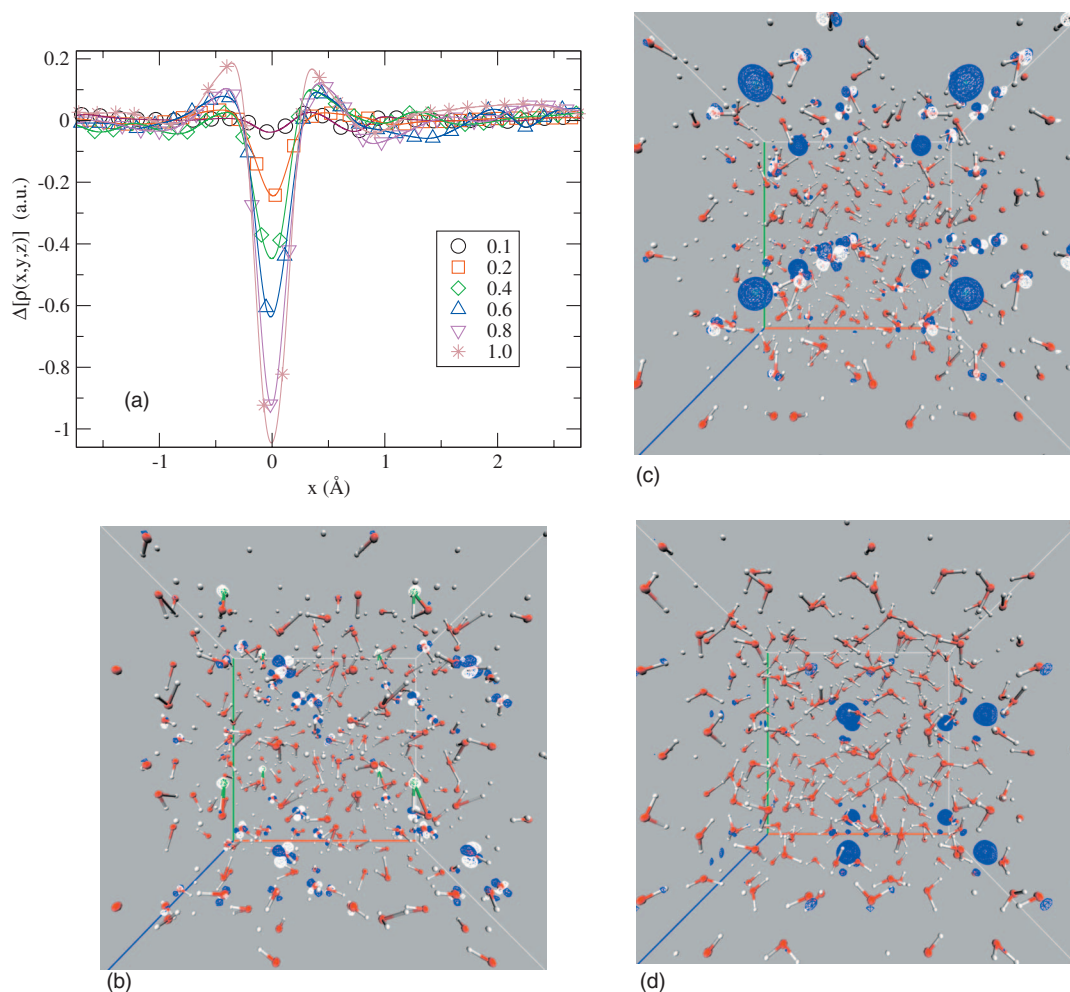


FIG. 3. (Color) (a) Integrated changes in electron density, $\Delta(x)=\int dydz[\rho(x,y,z)_n-\rho(x,y,z)_c]$, as a function of spatial coordinate x for the various values of q . ρ_n and ρ_c are the densities for the neutral and the charged systems, respectively. All charged species, Li^{q+} have been shifted to $x=0$. Symbols correspond to actual grid points, the continuous lines are cubic interpolations. [(b)–(d)] Isosurface plots of the electron density difference, $\rho(x,y,z)_n-\rho(x,y,z)_c$ (isovalue = ± 0.01 a.u., white ≤ 0 , blue ≥ 0), for $q=0.1, 0.6$, and 1.0 . Periodic boundary conditions apply; the prominent, eight blue spheres represent the (periodically replicated) changes in Li^{q+} densities, and some changes in water dipole moments are apparent too. See Sec. II B for technical details.

Cl^- ΔG_{hyd} calculations. The fact that the radius of Li^{q+} (and to some extent, other ions) changes with q in our DFT calculations also explains the discrepancy between AIMD and SPC/E $\langle dH(q)/dq \rangle_{q=0}$ values.

To compare AIMD predictions with experimental data, $\Delta G_{\text{Marcus}} + q\phi_q^{\text{SPC/E}} - 2C^{(0)}$ kcal/mol is found to be -137.0 kcal/mol,²¹ while $\Delta G_{\text{Tiss}} - q\phi_d^{\text{SPC/E}} - C^{(0)}$ kcal/mol = -133.2 kcal/mol (Ref. 22) (Table I). These values are similar to the SPC/E ΔG_{hyd} for Li^+ , and are 8.7 and 4.9 kcal/mol higher than the six-point AIMD prediction for a 32- H_2O simulation cell, respectively. The discrepancies with AIMD predictions may be due to numerical noise, PBE functional inaccuracies, or systematic uncertainties arising from the treatment of $|e|\phi$. Indeed, the discrepancy between SPC/E-augmented experimental values listed by Marcus²¹ and Tissandier *et al.*²² can also be taken as a measure of surface potential-related systematic ambiguity. This issue will be interrogated in the next subsection when we consider the anion Cl^- .

An optimal study of hydration free energy would include also the changes in water density due to the presence of salt cations and anions or water confinement inside nanopores.

We have therefore examined the effects of reducing the water density to 0.97 g/cm³. This small reduction in water density corresponds to the activity of water at $0.1M$ ion concentration, which is the typical concentration of K^+ ions in the cytoplasm of skeletal muscle cells and the typical concentration of Na^+ and Cl^- ions outside cells.⁵³ Table I shows that the small effect on ΔG_{hyd} due to water density changes is within the numerical uncertainty. This weak dependence is consistent with quasichemical theory analysis^{5,6} where contributions to ΔG_{hyd} are separated into inner hydration shell and outer shell contributions. In the “cluster” implementation of the theory,⁴ the former can be determined from gas phase cluster calculations scaled by water density, while the latter depends on the water dielectric constant, which is relatively independent of H_2O density. As pointed out by Varma and Rempe,⁵ since the dependence of free energies on water concentration is logarithmic, large changes in water density are required before there is an effect on ΔG_{hyd} .

B. Cl^- hydration free energy

Figures 6(a) and 6(b) depict the $g(r)$ between the classical force field Cl^{q-} (henceforth FF- Cl^{q-}) and the oxygen and

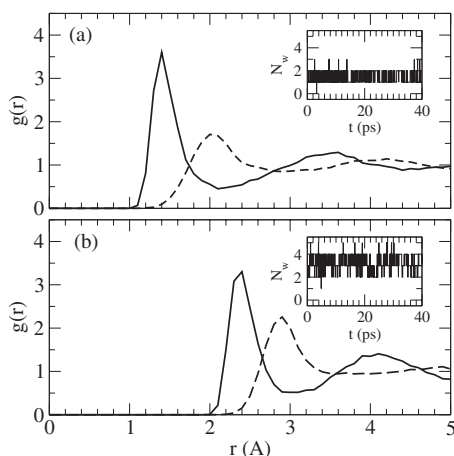


FIG. 4. Pair correlation functions $g(r)$ between Li^{q+} and the O (solid line) and H (dashed line) sites of H_2O molecules. (a) $q=0.21$; (b) $q=0.79$. The instantaneous hydration numbers are depicted in the insets.

proton sites of H_2O molecules at two q values. At $q=0.21$ (or even $q=0.4$), FF- Cl^{q-} is predominantly a hydrophobic sphere that excludes both O and H from its vicinity. Due to the sheer size of the Lennard-Jones sphere that represents Cl^{q-} , this solute is seen to substantially disrupt the water structure around it in the 32- H_2O simulation cell. Thus, in panel (b), the Cl-O $g(r)$ has dropped below 0.5 density units at $r \sim 5$ Å—unlike the case for Li^{q+} at small q [Fig. 4(a)]. At $q=0.79$, the ion forms hydrogen bonds with water; its $g_{\text{Cl-H}}(r)$ exhibits a peak at $r=2.2$ Å. At $q=1$ (not shown), we obtain a FF- Cl^{q-} hydration number of $N_w=5.4$, in good agreement with full AIMD simulations of PBE Cl^- in PBE water.^{56,57}

Figure 6(c) depicts the variation of $\langle dH(q)/dq \rangle_q$ FF- Cl^{q-} in PBE water as q varies.⁵⁸ To obtain ΔG_{hyd} for the PBE Cl^- ion, we further apply Eq. (7) to configurations sampled 0.1 ps apart along the AIMD trajectory. The differences between the instantaneous potential energies for FF- Cl^- and PBE Cl^- are found to be almost constant with an estimated standard deviation of 0.15 kcal/mol. This indicates that FF- Cl^- is an

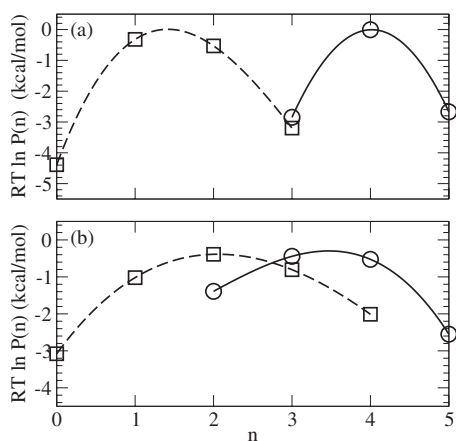


FIG. 5. Logarithm of the probability (P_n) of instantaneous hydration numbers (n) multiplied by thermal energy, in units of kcal/mol. (a) Li^{q+} ; (b) Ag^{q+} . Squares and dashed lines: $q=0.2$; circles and solid lines: $q=1.0$. n is determined by counting all water oxygen atoms within 2.08, 2.75, 2.90, and 2.92 Å of the four ions, respectively. These distances are determined by locating the first minimum in the ion-water $g(r)$.

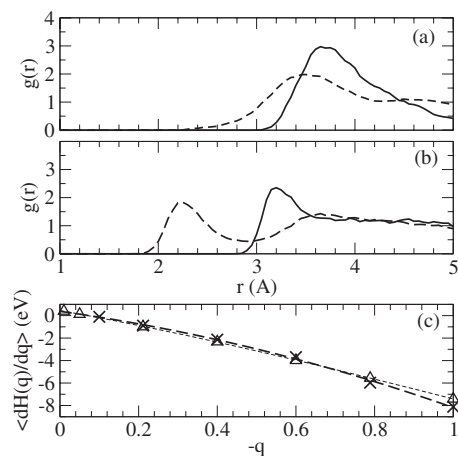


FIG. 6. [(a) and (b)] Pair correlation functions $g(r)$ between classical force field Cl^{q-} and the O (solid line) and H (dashed line) sites of PBE H_2O molecules. (a) $q=0.21$; (b) $q=0.79$. (c) $\langle dH(q)/dq \rangle_q$ for classical force field Cl^{q-} as q varies. Crosses and triangles are for AIMD and classical force field treatments of water in 32- H_2O simulation cells. The bare ion contributions, Ewald corrections, and electrostatic potential shift due to the quadrupole moment have been subtracted. The dashed lines are cubic least-squared fits.

excellent reference for the PBE Cl^- . After a cubic polynomial extrapolation to $q=0$ and applying a six-point integration formula, ΔG_{hyd} for the PBE Cl^- integrates to -76.6 ± 0.4 kcal/mol (Table I). A two-point Gaussian quadrature formula yields -79.0 ± 0.8 kcal/mol. As the latter is only exact for linear $\langle dH(q)/dq \rangle_q$, deviation from linearity in Fig. 6 indicates that a denser grid may be needed despite the constant radius of the FF- Cl sphere. This slight non-linearity is apparently due to water polarizability; corresponding six-point and two-point SPC/E calculations in 32-water simulation cells yield indistinguishable results. As $\langle dH(q)/dq \rangle_q$ is well fitted to a cubic polynomial in q and the trapezoidal integration rule is accurate for cubic polynomials, however, Fig. 6(c) strongly suggests that an integration formula higher order than the trapezoidal rule is not needed. Henceforth we report the six-point TI value.

Two postprocessing corrections for ΔG_{hyd} , unnecessary for Li^+ , need to be included here. (1) While the Li^+ PP is globally shrunk to zero, at $q=0$ FF- Cl^{q-} remains a Lennard-Jones sphere that displaces water. This gives rise to an entropic or “packing” penalty; the contribution is estimated to be 4.0 kcal/mol using SPC/E water model simulations. (2) Simulation cell size effects are more significant for Cl^- than for Li^+ , presumably because of the size of the Cl^{q-} sphere at small q [Fig. 6(a)]. When we perform purely classical force field simulations of a Cl^- ion in SPC/E water, we find that a 32- H_2O simulation cell overestimates ΔG_{hyd} by 3.3 kcal/mol compared to a 255- H_2O cell. This discrepancy is much larger than the numerical uncertainty. In contrast, these two cell sizes yield Li^+ ΔG_{hyd} that are within about 1 kcal/mol. The simulation cell size dependence has been estimated using a dielectric continuum approach in Ref. 9. Assuming AIMD exhibits Cl^- packing penalty and simulation cell size dependence similar to classical force field MD, we add a 7.3 kcal/mol correction to the AIMD result. The corrected AIMD Cl^- ΔG_{hyd} is listed in Table II. It is within 0.4 kcal/mol of

TABLE II. Cl^- hydration free energies. The asterisk denotes AIMD ΔG_{hyd} adjusted for finite simulation cell size and packing effects (see text). Also listed are ΔG_{hyd} for Li^+ plus Cl^- . The SPC/E results for Cl^- and Li^+/Cl^- contain the packing correction. H_2O densities and ΔG_{hyd} are in units of g/cm^3 and kcal/mol , respectively. Experimental values adjusted for surface potentials are depicted with a dagger; see text for details.

Ion	N_{water}	ρ_{water}	Quadrature	ΔG_{hyd}
Cl^-	32	1.00	2-pt	-79.0
Cl^-	32	1.00	6-pt	-76.6
Cl^-	32*	1.00	6-pt	-69.3
Cl^-	32 SPC/E	1.00	2-pt	-71.0
Cl^-	256 SPC/E	1.00	2-pt	-67.7
Cl^-	Expt. ^a	1.00	NA	-81.2
Cl^-	Expt. ^{a,†}	1.00	NA	-65.3
Cl^-	Expt. ^b	1.00	NA	-72.6
Cl^-	Expt. ^{b,†}	1.00	NA	-69.7
Li^+/Cl^-	32	1.00	6-pt	-197.6
Li^+/Cl^-	SPC/E	1.00	2-pt	-202.6
Li^+/Cl^-	Expt. ^a	1.00	NA	-202.3
Li^+/Cl^-	Expt. ^b	1.00	NA	-202.9

^aReference 21.

^bReference 22.

$\Delta G_{\text{Tiss}} - q\phi_d^{\text{SPC/E}} - C^{(0)}$ kcal/mol, and overestimates the magnitude of $\Delta G_{\text{Marcus}} + q\phi_q^{\text{SPC/E}} - 2C^{(0)}$ kcal/mol by 4.0 kcal/mol.

Adding ΔG_{hyd} of oppositely charged monovalent ions eliminates the systematic uncertainty due to surface potential contributions. The combined ΔG_{hyd} for Li^+ and Cl^- are within 4.7 and 5.3 kcal/mol of experimental data quoted in Table II, respectively.^{21,22} they underestimate those values only by about 2.3% and 2.6%. This sum, derived from Marcus²¹ and Tissandier *et al.*,²² are within 0.6 kcal/mol of each other, unlike in the cases of the isolated Li^+ and Cl^- ions where the two adjusted experimental data sets disagree by 3.8 and 4.4 kcal/mol, respectively. This suggests that the rather large, 8.7 kcal/mol discrepancy between AIMD ΔG_{hyd} and Marcus' data for Li^+ is partly due to the assignment of the SPC/E ϕ_q contribution to the surface potential. In contrast, data of Tissandier *et al.* for the isolated ions are in substantially better agreement with AIMD ΔG_{hyd} for both ions, suggesting that augmenting ΔG_{Tiss} with SPC/E ϕ_d is a reasonable approximation.

C. $\text{Ag} \rightarrow \text{Ag}^+$

In Fig. 7, $\text{Ag}-\text{H}_{\text{water}}$ and $\text{Ag}-\text{H}_{\text{water}}$ $g(r)$ are depicted for two selected values of q . Unlike Li, the Ag atomic core is not scaled with q , and Pauli repulsion ensures that no water molecule penetrates the Ag core region. Thus the $g(r)$ is not sharply structured at small q , and Ag^{q+} resembles a hydrophobic sphere as q decreases. For both q points, H_2O in the first hydration shells are highly labile; see the insets. The $\text{Ag}^+-\text{H}_2\text{O}$ $g(r)$ [Fig. 7(b)] yields a first shell hydration number $N_w=3.4$. The instantaneous hydration number distribution is depicted in Fig. 5. This N_w is qualitatively similar to the $N_w=4.0$ computed using AIMD and another exchange correlation functional.⁵⁹ Both these AIMD N_w values are in good agreement with experiments.^{60,61} In contrast, a recent classical force field model with parameters fitted to quantum

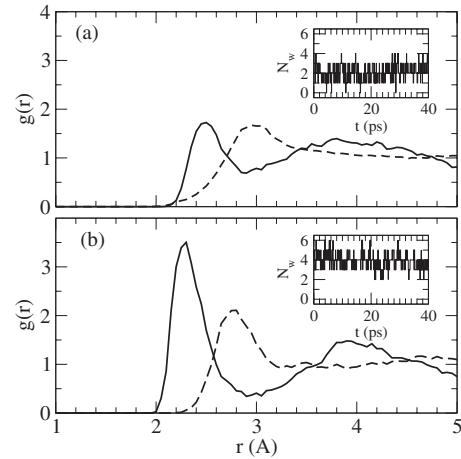


FIG. 7. Pair correlation functions $g(r)$ between Ag^{q+} and the O (solid line) and H (dashed line) sites of H_2O molecules. (a) $q=0.21$; (b) $q=1.00$. The instantaneous hydration numbers are depicted in the insets.

chemistry calculations has reported $N_w=6$.⁶² With the corrections (A)-(B) discussed earlier, a six-point trapezoidal rule integration, and a 1.6 kcal/mol packing correction estimated using classical force field simulations, we obtain $\Delta G_{\text{hyd}} = -119.8 \pm 0.4$ kcal/mol. This magnitude is 6.4 kcal/mol smaller than $\Delta G_{\text{Marcus}} + q\phi_q^{\text{SPC/E}} - 2C^{(0)}$ kcal/mol (Table III).²¹ The sum of AIMD Ag^+ and Cl^- ΔG_{hyd} , however, underestimates the experimental data²¹ by only 2.4 kcal/mol, or by 1.2%.

D. $\text{Ag}^+ + \text{Ni}^+ \rightarrow \text{Ag} + \text{Ni}^{2+}$

The details of Ni^{q+} hydration will be described elsewhere.⁶³ Here we focus on the change in ΔG_{hyd} as Ni^+ loses an electron. We use the PBE functional to compute $\langle dH(q)/dq \rangle_q$ at 0.1 ps intervals along the DFT+U AIMD trajectory with $U=4$ eV. Figure 8(b) shows that $\langle dH(q)/dq \rangle_q$ is fairly linear as q varies. With a six-point trapezoidal rule integration, Eq. (1) yields a change in ΔG_{hyd} of -365.5 ± 1.0 kcal/mol. A two-point integration predicts a

TABLE III. Ag^+ hydration free energies, and $\text{Ni}^+ \rightarrow \text{Ni}^{2+}$ hydration free energy changes. H_2O densities and ΔG_{hyd} are in units of g/cm^3 and kcal/mol , respectively. All simulations are based on the PBE functional, except that the DFT+U formalism with $U=4$ eV is applied for Ni predictions marked with an x . The asterisk denotes ΔG_{hyd} adjusted for packing effects. Experimental values adjusted for surface potentials are depicted with a dagger; see text for details.

Ion	N_{water}	ρ_{water}	Quadrature	ΔG_{hyd}
Ag^+	32	0.99	2-pt	-121.3
Ag^+	32	0.99	6-pt	-121.4
Ag^+	32*	0.99	6-pt	-119.8
Ag^+	Expt. ^a	1.00	NA	-102.7
Ag^+	Expt. ^{a,†}	1.00	NA	-126.2
Ag^+/Cl^-	32*	0.99	6-pt	-189.1
Ag^+/Cl^-	Expt. ^a	1.00	NA	-191.5
$\text{Ni}^+ \rightarrow \text{Ni}^{2+}$	32	0.99	2-pt	-365.4
$\text{Ni}^+ \rightarrow \text{Ni}^{2+}$	32	0.99	6-pt	-365.6
$\text{Ni}^+ \rightarrow \text{Ni}^{2+x}$	32	0.99	2-pt	-354.5
$\text{Ni}^+ \rightarrow \text{Ni}^{2+x}$	32	0.99	6-pt	-353.7

^aReference 21.

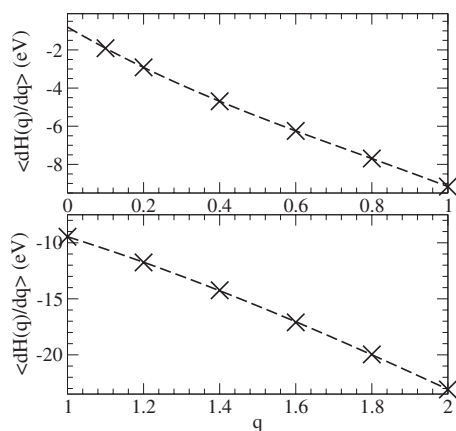


FIG. 8. $\langle dH(q)/dq \rangle_q$ for Ag^{q+} and Ni^{q+} as q varies. The bare ion contributions, Ewald corrections, and global shift in the electrostatic potential due to the quadrupole moment have been accounted for. The dashed lines are cubic least-squared fits.

similar -363.4 ± 2.4 kcal/mol. Unlike the calculations for Li^+ and Ag^+ , this system benefits from the fact that at “ λ ” $= (q-1)=0$, Ni^+ is still highly charged, and larger statistical uncertainty at small q is avoided. Nevertheless, due to the slower water dynamics around the more highly charged Ni^{q+} ion, sampling correlation times may be longer and our error bars for Ni^{2+} may be underestimated.

The electrochemical half cell reaction free energy consists of the change in ΔG_{hyd} plus the ionization potential (IP). The VASP PBE PP predicts the Ag IP to be 178.9 kcal/mol, while the first and second IP for Ni are predicted to be 160.6 and 492.9 kcal/mol, respectively. Adding the respective ΔG_{hyd} , Eqs. (5) and (6) yield ΔG of +57.5 and +76.0 kcal/mol, respectively. These individual half cell reaction ΔG have not yet been referenced to the standard hydrogen potential. The overall $Ag^+ + Ni^+ \rightarrow Ag + Ni^{2+}$ reaction, however, does not suffer from surface potential ambiguities. If we use the IP predicted using the PBE functional, the ΔG of this reaction becomes +18.5 kcal/mol, or +0.80 eV, in water. We stress that the pertinent Ag species is the silver atom suspended in water, not bulk silver metal.

PBE predictions for IP are, however, problematic. While our PP PBE method fortuitously predicts an Ag IP in reasonable agreement with the experimental value of 174.6 kcal/mol, the most accurate quantum chemistry method [CCSD(T)] with relativistic corrections, in fact, underestimates this value by ~ 1 eV.^{68,69} While the CCSD(T) method is accurate for the first IP of Ni,⁷⁰ our PP PBE approach severely overestimates the second Ni ionization potential measured at 418.7 kcal/mol.⁷¹

A more reasonable approach is to combine experimental IP and AIMD ΔG_{hyd} . This yields $\Delta G = +0.01$ eV for Eq. (4). The predicted value is significantly more endothermic than the -0.6 eV cited in the experimental radiolysis literature.^{31,64,65} That -0.6 eV value was derived by estimating the Ni^+ ΔG_{hyd} using a simple Pauling ionic radius and a dielectric continuum approximation;⁶⁵ as the authors stressed, ligand field effects, which can be a fraction of an eV for first row transition metal ions in water,⁶⁶ were neglected. AIMD ΔG_{hyd} calculations, free from these assump-

tions, should yield more accurate redox potentials for metal ions in unstable valence states encountered as transients in radiolysis experiments.^{64,65,67}

Finally, we note that the Ni^{2+} ΔG_{hyd} depends on whether the DFT+U approach is used in calculating $\langle dH(q)/dq \rangle_q$ along the AIMD trajectory. Setting $U=4(6)$ eV already decreases the gas phase $Ni^{2+}-(H_2O)_6$ cluster binding energy by ~ 0.5 eV (1.0 eV) without inducing noticeable changes in the geometry of the complex. Since the octahedral Ni^{2+} hydration shell is quite stable in liquid water, a similar change in the aqueous phase ΔG_{hyd} is expected if U varies by like amounts. We have indeed found that using DFT+U ($U=4$ eV) to compute $\langle dH(q)/dq \rangle_q$ decreases the solvation by roughly 12 kcal/mol, yielding a ΔG_{hyd} of -353.7 ± 1.0 kcal/mol. With this DFT+U ΔG_{hyd} , Eq. (4) becomes endothermic by +0.51 eV compared to the +0.01 eV predicted with PBE (i.e., $U=0$ eV). Whether PBE or DFT+U yields more accurate ΔG_{hyd} will be assessed in the future by comparison with high level quantum chemistry, new DFT functionals,⁷² or gas phase experimental values such as those reported for monovalent cations and anions.²²

The above analysis suggests that predicting redox potential of half cell electrochemical reactions of first row transition metal ions such as Ni^+ remains a challenge,^{34,35} and that reported redox values in the radiolysis literature^{64,65} may need to be extensively revised. We stress that our approach, which partitions redox potentials into hydration free energies and IP, circumvents DFT inaccuracies associated with IP predictions.

IV. CONCLUSIONS

We have applied AIMD simulations to compute the absolute hydration free energies of Li^+ , Cl^- , and Ag^+ . While some small contributions from packing (entropy) effects and simulation cell size dependences for anions still need to be estimated using classical force field based simulations, the dominant electrostatic contributions come from DFT and rigorous liquid state statistical mechanical methods.^{8,9,11,17}

To compare with experimental values, care must be taken to account for surface potential contributions which can be decomposed into water dipole and quadrupole (“second spherical moment”) contributions,^{17,20} $q(\phi_d + \phi_q)$. So far, the water-vapor interface surface potential has not been computed using AIMD/PBE. Nevertheless, the experimental data tabulated by Marcus²¹ and Tissandier *et al.*²² can be compared to AIMD values by adding $q\phi_q$ and subtracting $q\phi_d$ values estimated using the SPC/E water model, respectively. In both cases, we would be comparing with ΔG_{hyd} values fitted to the SPC/E water model; but to the extent that the SPC/E ϕ_d is an accurate physical quantity, comparing AIMD ΔG_{hyd} with $\Delta G_{\text{Tiss}} - \phi_d(\text{SPC/E})$ (plus a standard state correction $C^{(0)}$) should be model independent. With these caveats, we find that the AIMD ΔG_{hyd} for Li^+ and Cl^+ are within 4.9 (4%) and 0.4 kcal/mol (0.5%) of values of Tissandier *et al.* adjusted this way. The deviations from Marcus’ values,²¹ compiled after removing surface potential and standard state contributions, are larger, probably due to uncertainties in ϕ_q estimates. The sum of ΔG_{hyd} for the Li^+/Cl^- ion pair, where

surface potential effects cancel, agree with the two sets of experimental values to within 2.3% and 2.6%, respectively.^{21,22} The Ag⁺/Cl⁻ ion pair has a combined ΔG_{hyd} within 1.2% of Marcus' data.

We also compute the change in ΔG_{hyd} associated with Ni⁺ being oxidized to Ni²⁺. Coupled with the hydration free energy of Ag⁺ and experimental ionization potential values, we arrive at a free energy change of 0.01 eV (PBE) and 0.51 eV (DFT+U, $U=4$ eV) for the Ag⁺+Ni⁺→Ag(atom)+Ni²⁺ reaction in water. Whether PBE or DFT+U yields more accurate ΔG_{hyd} will be assessed in the future by comparison with high level quantum chemistry, new DFT functionals, or experimental values. This calculation is pertinent to predicting the redox potential of unstable Ni⁺ ions. The Ni⁺ oxidation potential often cited in the radiolysis experimental literature actually contains a theoretical hydration free energy estimate based on the Ni⁺ Pauling radius, and it does not account for ligand field effects.^{64,65} Our results suggest that such reported values may need to be re-examined with the more accurate AIMD approach.

Even without more accurate determination of surface potentials, our formalism can be applied to predict the AIMD ΔG_{hyd} difference between like-charged ions such as Na⁺ and K⁺, which is relevant to understanding mechanisms of selective ion binding. Our work also paves the way for AIMD calculations of the hydration free energies of more complex ions and of ions at water-material interfaces, inside carbon nanotubes where material polarizability is significant,¹⁹ and in inhomogeneous aqueous media in general. Further work on elucidating the surface potential entirely with AIMD methods, systematic investigation of the U dependence of hydration free energy when DFT+U is applied, and comparison with other functionals [e.g., BLYP (Ref. 73)] and AIMD packages [e.g., CPMD (Ref. 40)] will be pursued in the future.

ACKNOWLEDGMENTS

K.L. thanks Tina Nenoff and Matt Petersen for useful discussions. S.B.R. acknowledges funding by the National Institutes of Health through the NIH Road Map for Medical Research. O.A.v.L. acknowledges support from the SNL Truman Program LDRD under Project No. 120209. This work was also supported by the Department of Energy under Contract No. DE-AC04-94AL85000, by Sandia's LDRD program. Sandia is a multiprogram laboratory operated by Sandia Corporation, a Lockheed Martin Co., for the U.S. Department of Energy.

¹R. T. Cygan, C. J. Brinker, M. D. Nyman, K. Leung, and S. B. Rempe, *MRS Bull.* **33**, 42 (2007).

²Examples include F. Brugé, M. Bernasconi, and M. Parrinello, *J. Am. Chem. Soc.* **121**, 10883 (1999); S. B. Rempe and L. R. Pratt, *Fluid Phase Equilib.* **183**, 121 (2001); L. M. Ramaniah, M. Bernasconi, and M. Parrinello, *J. Chem. Phys.* **111**, 1587 (1999); E. Schwegler, G. Galli, and F. Gygi, *Chem. Phys. Lett.* **342**, 434 (2001); I.-F. Kuo and D. J. Tobias, *J. Phys. Chem. B* **105**, 5827 (2001); S. Rauegi and M. L. Klein, *J. Am. Chem. Soc.* **123**, 9484 (2001); *J. Chem. Phys.* **116**, 196 (2002); K. Leung and S. B. Rempe, *J. Am. Chem. Soc.* **126**, 344 (2004); S. B. Rempe, D. Asthagiri, and L. R. Pratt, *Phys. Chem. Chem. Phys.* **6**, 1966 (2004); S. Varma and S. B. Rempe, *Biophys. Chem.* **124**, 192 (2006); T. W. Whitfield, S. Varma, E. Harder, G. Lamoureux, S. B. Rempe, and B.

Roux, *J. Chem. Theor. Comput.* **3**, 2068 (2007); K. Leung, I. M. B. Nielsen, and I. Kurtz, *J. Phys. Chem. B* **111**, 4453 (2007).

³S. B. Rempe, L. R. Pratt, G. Hummer, J. D. Kress, R. L. Martin, and A. Redondo, *J. Am. Chem. Soc.* **122**, 966 (2000).

⁴D. Sabo, S. Varma, M. G. Martin, and S. B. Rempe, *J. Phys. Chem. B* **112**, 867 (2008).

⁵S. Varma and S. B. Rempe, *J. Am. Chem. Soc.* **130**, 15405 (2008).

⁶L. R. Pratt and R. A. LaViolette, *Mol. Phys.* **94**, 909 (1998); L. R. Pratt and S. B. Rempe, in *Simulation and Theory of Electrostatic Interactions in Solution*, edited by L. R. Pratt and G. Hummer (AIP, New York, 1999), pp. 172–201; T. L. Beck, M. E. Paulaitis, and L. R. Pratt, *The Potential Distribution Theorem: Models of Molecular Solutions* (Cambridge University Press, New York, 2006); S. Varma and S. B. Rempe, *Biophysical J.* **93**, 1093 (2007); S. Varma, D. Sabo, and S. B. Rempe, *J. Molec. Bio.* **376**, 13 (2008).

⁷O. A. von Lilienfeld and M. E. Tuckerman, *J. Chem. Theory Comput.* **3**, 1083 (2007); *J. Chem. Theory Comput.* **125**, 154104 (2006); O. A. von Lilienfeld, R. D. Lins, and U. Rothlisberger, *Phys. Rev. Lett.* **95**, 153002 (2005).

⁸G. Hummer, L. R. Pratt, and A. E. Garcia, *J. Phys. Chem.* **100**, 1206 (1996).

⁹G. Hummer, L. R. Pratt, and A. E. Garcia, *J. Chem. Phys.* **107**, 9275 (1997).

¹⁰S. Rajamani, T. Ghosh, and S. Garde, *J. Chem. Phys.* **120**, 4457 (2004).

¹¹G. Hummer, L. R. Pratt, A. E. Garcia, B. J. Berne, and S. W. Rick, *J. Phys. Chem. B* **101**, 3017 (1997); G. Hummer, L. R. Pratt, and A. E. Garcia, *J. Phys. Chem. A* **102**, 7885 (1998); H. S. Ashbaugh and R. H. Wood, *J. Chem. Phys.* **106**, 8135 (1997); T. Darden, D. Pearlman, and L. G. Pedersen, *ibid.* **109**, 10921 (1998); R. M. Lynden-Bell and J. C. Rasaiah, *ibid.* **107**, 1981 (1997); F. Figueirido, G. S. Del Buono, and R. M. Levy, *J. Phys. Chem. B* **101**, 5622 (1997); P. H. Hünenberger and J. A. McCammon, *J. Chem. Phys.* **110**, 1856 (1999); A. Grossfield, P.-Y. Ren, and J. W. Ponder, *J. Am. Chem. Soc.* **125**, 15671 (2003); H. S. Ashbaugh and D. Asthagiri, *J. Chem. Phys.* **129**, 204501 (2008).

¹²J. G. Kirkwood, *J. Chem. Phys.* **3**, 300 (1935).

¹³M. P. Allen and D. J. Tildesley, *Computer Simulation of Liquids* (Oxford University Press, New York, 1987).

¹⁴P. A. Kollman, *Chem. Rev. (Washington, D.C.)* **93**, 2395 (1993).

¹⁵H. J. C. Berendsen, J. R. Gridera, and T. P. Straatsma, *J. Phys. Chem.* **91**, 6269 (1987).

¹⁶Real space truncation of Coulomb interactions lead to other problems. As our focus is AIMD simulations based on DFT calculations using periodic boundary conditions, which almost universally apply Ewald summations, real space truncations will not be considered further herein.

¹⁷L. R. Pratt, *J. Phys. Chem.* **96**, 25 (1992); M. A. Wilson, A. Pohorille, and L. R. Pratt, *J. Chem. Phys.* **88**, 3281 (1988); M. A. Wilson, A. Pohorille, and L. R. Pratt, *J. Phys. Chem.* **91**, 4873 (1987); Y. Zhou, G. Stell, and H. L. Friedman, *J. Chem. Phys.* **89**, 3836 (1988).

¹⁸V. P. Sokhan and D. J. Tildesley, *Mol. Phys.* **92**, 625 (1997).

¹⁹K. Leung and M. Marsman, *J. Chem. Phys.* **127**, 154722 (2007) (Our present work closely follows this preceding work, but uses slightly different notations. In particular, instead of “second spherical moments,” we use the “quadrupole moments” more widely used in the liquid state literature.)

²⁰V. R. Saunders, C. Freyria-Fava, R. Dovesi, L. Salasco, and C. Roetti, *Mol. Phys.* **77**, 629 (1992).

²¹Y. Marcus, *Biophys. Chem.* **51**, 111 (1994), and references therein.

²²M. D. Tissandier, K. A. Cowen, W. Y. Feng, E. Grunlach, M. H. Cohen, A. D. Earhart, J. V. Coe, and T. R. Tuttle, *J. Phys. Chem. A* **102**, 7787 (1998).

²³J. P. Perdew, K. Burke, and M. Ernzerhof, *Phys. Rev. Lett.* **77**, 3865 (1996).

²⁴L. X. Dang and T.-M. Chang, *J. Phys. Chem. B* **106**, 235 (2002).

²⁵I. F. W. Kuo and C. J. Mundy, *Science* **303**, 658 (2004).

²⁶M. J. McGrath, J. I. Siepmann, I. F. W. Kuo, and C. J. Mundy, *Mol. Phys.* **104**, 3619 (2006).

²⁷C. G. Barraclough, P. T. McTigue, and Y. L. Ng, *J. Electroanal. Chem.* **320**, 9 (1992).

²⁸E. N. Brodskaya and V. V. Zakharov, *J. Chem. Phys.* **102**, 4595 (1995).

²⁹Our value for the SPC/E water ϕ_q may be slightly different from values reported in water-vapor interface simulations because of possible small variations in the water density in interfacial simulation cells. Note also that Ref. 18 appears to have misquoted the value of ϕ_d for the TIP4P

- water from Ref. 28, and that the ϕ_d for this model reported in Ref. 17 was computed at $T=325$ K, not the $T=300$ K of Ref. 28.
- ³⁰ C. P. Kelly, C. J. Cramer, and D. G. Truhlar, *J. Phys. Chem. B* **110**, 16066 (2006).
- ³¹ Z. Zhang, T. M. Nenoff, J. Huang, D. T. Berry, and P. P. Provencio, *J. Phys. Chem. C* **113**, 1155 (2009).
- ³² B. G. Ershov, E. Janata, and A. Henglein, *J. Phys. Chem.* **98**, 7619 (1994); J. Belloni, *Catal. Today* **113**, 141 (2006).
- ³³ D. Asthagiri, L. R. Pratt, and H. S. Ashbaugh, *J. Chem. Phys.* **119**, 2702 (2003).
- ³⁴ X. C. Zeng, H. Hu, X. Q. Hu, A. J. Cohen, and W. T. Yang, *J. Chem. Phys.* **128**, 124510 (2008).
- ³⁵ J. VandeVondele, R. Ayala, M. Sulpizi, and M. Sprik, *J. Electroanal. Chem.* **607**, 113 (2007); Y. Tateyama, J. Blumberger, T. Ohno, and M. Sprik, *J. Chem. Phys.* **126**, 204506 (2007).
- ³⁶ G. Kresse and J. Furthmüller, *Phys. Rev. B* **54**, 11169 (1996); *Comput. Mater. Sci.* **6**, 15 (1996).
- ³⁷ P. E. Blöchl, *Phys. Rev. B* **50**, 17953 (1994).
- ³⁸ The VASP implementation is discussed in G. Kresse and D. Joubert, *Phys. Rev. B* **59**, 1758 (1999).
- ³⁹ E. Schwegler, J. C. Grossman, F. Gygi, and G. Galli, *J. Chem. Phys.* **121**, 5400 (2004); P. H.-L. Sit and N. Marzari, *ibid.* **122**, 204510 (2005); S. B. Rempe, T. R. Mattsson, and K. Leung, *Phys. Chem. Chem. Phys.* **10**, 4685 (2008).
- ⁴⁰ CPMD, <http://www.cpmid.org>, Copyright IBM Corp 1990–2008, Copyright MPI für Festkörperforschung Stuttgart 1997–2001.
- ⁴¹ M. Krack, *Theor. Chem. Acc.* **114**, 145 (2005).
- ⁴² We have avoided directly computing the integrand at $q=0$ because the AIMD trajectories may be too short to adequately sample the small q regions. $\langle dH(q)/dq \rangle$ at such q values exhibit larger statistical fluctuations. To test the extrapolation to $q=0$, we have conducted classical force field TI simulations with much longer trajectory lengths but otherwise identical TI protocol and compared to $\langle dH(q)/dq \rangle$ directly computed at $q=0$. These simulations indicate that a cubic fit using our set of $6q$ values yields a good approximation to the $q=0$ integrand.
- ⁴³ Recall that this contribution is estimated using maximally localized Wannier functions to decompose the total electron density into individual water contributions (Ref. 19). As an additional test, we have taken the nuclear configuration of each of the 32 individual water molecules in an AIMD snapshot, computed the individual water ϕ_q contribution in the absence of other water molecules, added them, and compared the result with the global ϕ_q correction computed with all $32\text{H}_2\text{O}$ simultaneously present in the same cell. Even though the individual H_2O approach neglects many-water effects, the two ϕ_q contributions computed are within 1%, or 1 kcal/mol, of each other.
- ⁴⁴ N. Marzari and D. Vanderbilt, *Phys. Rev. B* **56**, 12847 (1997).
- ⁴⁵ This behavior is not universal. Attempting to put a partial (or an entire) $2s$ electron on the Li^+ PP to yield Li^{q+} in water, as opposed to globally scaling that PP by the factor q , results in the partial electron leaving the vicinity of Li^{q+} and becoming solvated as an excess electron in water. In other words, if we were interested in the $\text{Li Li} \rightarrow \text{Li}^+$ half cell reaction, a more complex λ -paths would have been needed. Spontaneous ejection of electrons does not happen with Ag or Ni^+ , both of which are less electropositive than Li.
- ⁴⁶ V. I. Anisimov, J. Zaanen, and O. K. Andersen, *Phys. Rev. B* **44**, 943 (1991); A. I. Liechtenstein, V. I. Anisimov, and J. Zaanen, *ibid.* **52**, R5467 (1995). For details of DFT+U implementation, see Ref. 47.
- ⁴⁷ K. Leung and C. J. Medforth, *J. Chem. Phys.* **126**, 024501 (2007).
- ⁴⁸ P. H. L. Sit, M. Cococcioni, and N. Marzari, *J. Electroanal. Chem.* **607**, 107 (2007).
- ⁴⁹ A. D. Becke, *J. Chem. Phys.* **98**, 1372 (1993); **98**, 5648 (1993); C. T. Lee, W. T. Yang, and R. G. Parr, *Phys. Rev. B* **37**, 785 (1988).
- ⁵⁰ The $6\text{-}311+\text{G}(d,p)$ basis also yields a PBE binding energy of 15.7 eV. As discussed in Ref. 47, this basis and the plane-wave/PAW method used in VASP yield results that are in good agreement.
- ⁵¹ It may be argued that the trajectory length is short and the sampled configurations are correlated, which may underestimate the numerical noise. Hence we have tested the uncertainty using classical force fields and much longer trajectories. With otherwise identical parameters ($32\text{H}_2\text{O}$, 0.1 ps sampling intervals, extrapolation to $q=0$), a 400 ps SPC/E trajectory reveals that, on average, a 40 ps segment of the trajectory exhibits 0.44 and 0.52 kcal/mol standard deviations for the six- and two-point TI scheme, respectively. Normally a six-point TI should exhibit far less noise than a two-point one; in the present case, the extrapolation to $q=0$ required for the six-point trapezoidal rule has introduced additional uncertainties. These uncertainties in SPC/E simulations are indeed comparable to and even smaller than the standard deviations estimated for the 40 ps AIMD trajectories.
- ⁵² G. Hummer, L. R. Pratt, and A. E. Garcia, *J. Am. Chem. Soc.* **119**, 8523 (1997).
- ⁵³ B. Hille, *Ionic Channels of Excitable Membranes* (Sinauer Associates, Sunderland, MA, 2001).
- ⁵⁴ A. Paliwal, D. Asthagiri, L. R. Pratt, H. S. Ashbaugh, and M. E. Paulaitis, *J. Chem. Phys.* **124**, 224502 (2006).
- ⁵⁵ G. Hummer, *Mol. Simul.* **28**, 81 (2002).
- ⁵⁶ P. Jungwirth and D. J. Tobias, *J. Phys. Chem. A* **106**, 379 (2002).
- ⁵⁷ K. Leung and S. B. Rempe, *Phys. Chem. Chem. Phys.* **8**, 2153 (2006).
- ⁵⁸ While the isolated Cl^- ion as predicted by PBE may not be stable in vacuum, within our periodic boundary condition simulations, Cl^- has a well defined total energy and a HOMO-LUMO gap over a large range of simulation cell sizes.
- ⁵⁹ J. Blumberger, L. Bernasconi, I. Tavernelli, R. Vuilleumier, and M. Sprik, *J. Am. Chem. Soc.* **126**, 3928 (2004).
- ⁶⁰ J. Texter, J. J. Hastreiter, and J. L. Hall, *J. Phys. Chem.* **87**, 4690 (1983).
- ⁶¹ M. Sandström, G. W. Neilson, G. Johansson, and T. Yamaguchi, *J. Phys. C: Solid State Phys.* **18**, L1115 (1985).
- ⁶² V. Dubois, P. Archirel, and A. Boutin, *J. Phys. Chem. B* **105**, 9363 (2001).
- ⁶³ K. Leung and T. M. Nenoff (unpublished).
- ⁶⁴ M. Breitenkamp, A. Henglein, and J. Lilie, *Ber. Bunsenges. Phys. Chem.* **80**, 973 (1976).
- ⁶⁵ J. H. Baxendale and R. S. Dixon, *Z. Phys. Chem. (Munich)* **43**, 161 (1964).
- ⁶⁶ D. Asthagiri, L. R. Pratt, M. E. Paulaitis, and S. B. Rempe, *J. Am. Chem. Soc.* **126**, 1285 (2004).
- ⁶⁷ J. H. Baxendale, J. P. Keene, and D. A. Stott, *Chem. Commun. (Cambridge)* **20**, 715 (1996).
- ⁶⁸ M. N. Huda and A. K. Ray, *Eur. Phys. J. D* **22**, 217 (2003).
- ⁶⁹ C. E. Moore, *Natl. Stand. Ref. Data. Ser., Natl. Bur. Stand. (U. S.)* **35** (1971).
- ⁷⁰ N. B. Balabanov and K. A. Peterson, *J. Chem. Phys.* **125**, 074110 (2006).
- ⁷¹ A. G. Shenstone, *J. Res. Natl. Bur. Stand.* **74A**, 80 (1970).
- ⁷² Y. Zhao and D. G. Truhlar, *J. Chem. Phys.* **125**, 194101 (2006).
- ⁷³ A. D. Becke, *Phys. Rev. A* **38**, 3098 (1988).